European Journal of Radiology 113 (2019) 245–250

Contents lists available at ScienceDirect

European Journal of Radiology

journal homepage: www.elsevier.com/locate/ejrad

Texture analysis of myocardial infarction in CT: Comparison with visual analysis and impact of iterative reconstruction

Manoj Mannil[a,*], Jochen von Spiczak[a], Urs J. Muehlematter[a], Arjun Thanabalasingam[a], Dagmar I. Keller[c], Robert Manka[a,b,d], Hatem Alkadhi[a]

[a] Institute of Diagnostic and Interventional Radiology, University Hospital Zurich, University of Zurich, Raemistr. 100, CH-8091 Zurich, Switzerland
[b] Department of Cardiology, University Heart Center, University Hospital Zurich, University of Zurich, Raemistr. 100, 8091 Zurich, Switzerland
[c] Institute for Emergency Medicine, University Hospital Zurich, University of Zurich, Switzerland
[d] Institute for Biomedical Engineering, University and ETH Zurich Gloriastrasse 35, 8092 Zurich, Switzerland

ARTICLE INFO

Keywords:
Texture analysis
Myocardial infarction
Computed tomography
Machine learning
Iterative reconstruction

ABSTRACT

Objectives: To compare texture analysis (TA) with subjective visual diagnosis of myocardial infarction (MI) in cardiac computed tomography (CT) and to evaluate the impact of iterative reconstruction (IR).
Methods: Ten patients (4 women, mean age 68 ± 11 years) with confirmed chronic MI and 20 controls (8 women, mean age 52 ± 11 years) with no cardiac abnormality underwent contrast-enhanced cardiac CT with the same protocol. Images were reconstructed with filtered back projection (FBP) and with advanced modeled IR at strength levels 3–5. Subjective diagnosis of MI was made by three independent, blinded readers with different experience levels. Classification of MI was performed using machine learning–based decision tree models for the entire data set and after splitting into training and test data to avoid overfitting.
Results: Subjective visual analysis for diagnosis of MI showed excellent intrareader (kappa: 0.93) but poor interreader agreement (kappa: 0.3), with variable performance at different image reconstructions. TA showed high performance for all image reconstructions (correct classifications: 94%–97%, areas under the curve: 0.94–0.99). After splitting into training and test data, overall lower performances were observed, with best results for IR at level 5 (correct classifications: 73%, area under the curve: 0.65).
Conclusions: As compared with subjective, nonreliable visual analysis of inexperienced readers, TA enables objective and reproducible diagnosis of chronic MI in cardiac CT with higher accuracy. IR has a considerable impact on both subjective and objective image analysis.

1. Introduction

Ischemic heart disease accounts for approximately 10% of annual deaths worldwide, with myocardial infarction (MI) representing the leading cause of mortality [1]. Coronary atherosclerosis with subsequent plaque rupture and vessel occlusion is considered the main pathophysiological mechanism for MI [2].

Coronary computed tomography angiography (CTA) enables the noninvasive detection of coronary atherosclerosis and obstructive coronary artery disease (CAD). Having an excellent negative predictive value [3], coronary CTA has been recommended in patients with a low to intermediate pretest probability of CAD [4,5]. In addition to the coronary arteries, CT has also been tested for evaluation of myocardial ischemia and infarction, being visible in contrast-enhanced CT as a focal area of decreased attenuation. In contrast to magnetic resonance (MR) imaging, which is the gold standard modality for assessment of the myocardium, the accuracy of CT falls short [6,7]. This is particularly true in CT coronary angiography images performed during the arterial first pass of contrast media. The main reason for this shortcoming is the limited contrast resolution of CT, which researchers have tried to overcome with higher volumes of administered contrast medium, with higher radiation doses for improving the contrast-to-noise ratio, or by employing dual-energy CT to improve the visualization of MI [8].

Abbreviations: ADMIRE, advanced modeled iterative reconstruction; AUC, area under the curve; CT, computed tomography; CTA, computed tomography angiography; DICOM, digital imaging and communications in medicine; ECG, electrocardiography; FBP, filtered back projection; GLCM, gray-level co-occurrence matrix; IR, iterative reconstruction; MI, myocardial infarction; RLM, run-length matrix; ROC, receiver-operating characteristic; TA, texture analysis

* Corresponding author.
E-mail address: manoj.mannil@usz.ch (M. Mannil).

https://doi.org/10.1016/j.ejrad.2019.02.037
Received 19 October 2018; Received in revised form 25 February 2019; Accepted 26 February 2019

For restricting ionizing radiation from CT, several methods have been recently developed and implemented, including tube current modulation, lowering and optimizing tube voltage, and the use of iterative reconstructions (IR). While IR can be used to lower the radiation dose, it is also known that IR may change the appearance and texture of CT images, potentially masking imaging findings, which occurs particularly when reducing the radiation dose [9,10].

Texture analysis (TA) refers to an objective and quantitative set of metrics calculated in image processing for quantifying the texture of images. TA has the potential for objective quantification of tissue and disease characteristics and can also be used for detecting abnormalities in radiological images that cannot be depicted by the readers' eyes alone [11–14]. Thus, TA could have the potential to detect MI in cardiac CT images, which is potentially overlooked in a pure visual analysis. This holds particularly true when infarcts are small, readers have limited experience, or readers do not pay enough attention to the myocardium.

The purpose of this study was twofold: first, to compare machine learning–based TA with subjective visual diagnosis of MI in cardiac CT and, second, to evaluate the impact of IR on the results of both subjective and objective image analysis.

2. Materials and methods

2.1. Study patients

Between October 2016 and March 2017, we included 10 patients (4 women, 6 men; mean age 68 ± 11 years; range 53–87 years) with 11 MI into this study (Table 1). All patients underwent clinically indicated electrocardiography (ECG)–gated, contrast-enhanced coronary CTA in our emergency department. We included patients with chronic MI, defined as being older than one year since initial presentation [15]. Diagnosis of chronic MI was based in all patients on ECG, laboratory biomarkers, and catheter coronary angiography findings at previous, initial presentation. The extent of MI was determined by the following cross-sectional imaging modalities: MR imaging (n = 6), single-photon emission CT (n = 1), and positron emission tomography (n = 3). MI was transmural in one (9%) and subendocardial in 10 cases (92%) and was restricted to one myocardial segment in all patients (according to the American Heart Association classification scheme [16]). We excluded patients with compromised image quality, deviating image acquisition parameters and uncertain final diagnosis.

For the control population, additional 20 patients (8 women, 12 men; mean age 52 ± 11 years; range 24–71 years) who underwent the same CT protocol on the same CT scanner during the same time period showing no clinical or imaging evidence of CAD and no myocardial abnormality were included. The indication for coronary CTA in this group, hereafter called *controls*, was atypical chest pain at a low pretest probability of CAD.

This retrospective study had institutional review board and local ethics committee approval; written informed consent requirement was waived.

Table 1
Descriptive statistics of controls and patients with MI.

	Controls	Patients With MI
n (instances)	20 (20)	10 (11)
Age (years)	52 ± 11	68 ± 11
Sex	40% female 60% male	40% female 60% male
Agatston score	0	1123 ± 185*
Current/history of smoking	25%	44%*
Hypertension	5%	46%*
Hypercholesterolemia	25%	36%*
Diabetes	5%	36%*
Overweight (BMI > 30 kg/m^2)	5%	18%*

MI = myocardial infarction; BMI = body mass index. *($p < 0.01$).

2.2. CT data acquisition and postprocessing

All examinations were performed on a third-generation dual-source CT scanner (SOMATOM Force, Siemens Healthineers, Forchheim, Germany). Acquisition parameters were as follows: slice collimation 2 × 96 × 0.6 mm, slice acquisition 2 × 192 × 0.6 mm using the z-flying focal spot, gantry rotation time 250 ms, reference tube voltage 100 kVp using automated tube voltage selection (CAREkV, Siemens), and quality reference tube current-time product 200 mAs per rotation using automated exposure control (CAREDose, Siemens). Data acquisition synchronized to the ECG. The contrast media protocol was as follows: first, 50–75 mL nonionic iodinated contrast material (iopromidum, Ultravist 370, 370 mg/mL, Bayer, Leverkusen, Germany) with a flow rate of 5–6 mL/sec, depending on the body mass index of the patients, was injected into an antecubital vein followed by the same volume consisting of 20% contrast media and 80% saline solution.

Axial CT images were reconstructed with a slice thickness of 0.6 mm (increment 0.4 mm) using a soft-tissue convolution kernel (Bv36). Four different reconstructions were performed for in each control and patient: filtered back projection (FBP) and advanced modeled IR (ADMIRE) at strength levels 3, 4, and 5 (Fig. 1). From these images, short-axis reformations of the left ventricle (LV) were reformatted at a slice thickness of 5 mm, as previously shown [17], using commercially available postprocessing software (CT Cardiac Function, syngo.via, Siemens).

In patients with MI, short-axis images showing the largest extent of infarction were chosen, while in controls, short-axis images in midventricular myocardium were selected. Reformatted images were all anonymized and stored in digital imaging and communications in medicine (DICOM) file format.

As several TA features require identical spatial resolution and pixel size to be comparable, all images were rescaled according to the pixel spacing values obtained from the DICOM header. Rescaling was performed using an in-house MATLAB routine to the coarsest in-plane resolution of 0.3 × 0.3 mm^2.

2.3. Subjective visual image analysis

A total of 120 image data sets (30 patients × four reconstructions) were analyzed for the presence or absence of MI by three blinded and independent readers (R1, having one year of experience in cardiovascular imaging, and R2, having two years of experience in cardiovascular

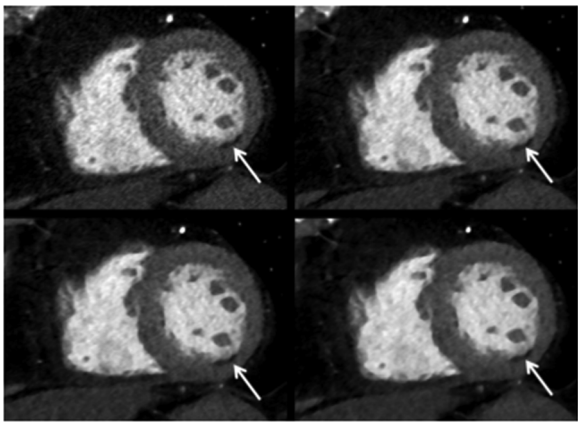

Fig. 1. Short-axis reformations (slice thickness = 5 mm) of a coronary CTA examination in a 77-year-old female patient with subendocardial inferior midventricular myocardial infarction (arrow) using (A) filtered back projection, (B) advanced modeled iterative reconstruction (ADMIRE) strength level 3, (C) ADMIRE strength level 4, and (D) ADMIRE strength level 5.

imaging, and R3, having six years of experience in cardiovascular imaging) to determine the interreader agreement. R1 and R2 readers were radiology residents who read cardiac CT examinations during after hour and night shifts during their emergency radiology rotation. After an interval of 4 weeks, R2 repeated the readout to determine the intrareader agreement. All readers were presented all axial source images and short-axis reformations for readout. To re-create a real-life scenario, CT images were initially presented at fixed window settings (width 360; level 70), and readers were allowed to change the settings according to their individual preferences. All readers were blinded to patient information, results from the other readers, results of all the other imaging tests including cross-sectional imaging, and the final diagnosis.

2.4. Texture analysis

TA was performed using a freely available software package (MaZda, version 4.6, Institute of Electronics, Technical University of Lodz, Lodz, Poland) [18]. Gray-level normalization was performed between the mean and three standard deviations (" ± 3σ" method), which is done for correcting small technical variations [19].

Free-hand regions of interest (ROIs) were drawn on short-axis reformations including the LV myocardium (and carefully excluding the blood pool) by two other readers (R3, having 4 years of experience in cardiovascular imaging, and R4, having 2 years of experience in cardiovascular imaging) to determine the interreader agreement and by R3 twice to determine the intrareader agreement of TA. Overall, 308 TA features were computed per ROI.

2.5. TA feature selection

Feature selection was performed on the 308 TA features by removing those showing a reduced intra- and interreader agreement. For doing so, intraclass correlation coefficients (ICCs) were calculated for each pair of variables. According to Landis and Koch, ICCs of 0.61–0.8 were interpreted as substantial and 0.81–1.00 as excellent agreement [20]. We excluded TA features with an ICC < 0.6 from further analyses.

2.6. Statistical analysis

Continuous variables were expressed as means ± standard deviation or medians with interquartile ranges, as appropriate. Categorical variables were expressed as frequencies or percentages. The intra- and interreader agreement for subjective visual image analysis regarding the presence or absence of MI was calculated using Cohen's kappa. The subjective visual analysis findings were compared with the reference standard, and sensitivity and specificity were calculated.

For quantitative image analysis, TA features were tested in four separate models for each reconstruction type (FBP, ADMIRE strength level 3–5) regarding the discriminatory power of TA features in the identification of MI. For this purpose, we used in each data set the machine learning–based decision tree classifier C4.5 (J48, Weka). The decision tree classifier is an implementation of the C4.5 classifier which uses pruning for further dimension reduction. The confidence factor was set to 0.25. The number of folds was set 3 and minimum description length (MDL) correction was used.

Results of the four C4.5 decision tree models were compared regarding correctly/incorrectly classified instances, mean absolute error, true-/false-positive rates, precision, and the area under the curve (AUC) from the receiver-operating characteristic analysis. Because of the limited cohort size (n = 30 patients, n = 120 datasets), we performed classification analyses twice: First, the entire data set was used for training and testing the machine learning–based decision trees. Then, we used a percentage split at random in the recommended ratio of 2/3 (66.7%, n = 20 / image reconstruction) training set and tested on the remaining 1/3 (33.3%, n = 10 / image reconstruction) to account for overfitting [21]. Data mining and machine learning algorithms were performed using open-source software (WEKA, University of Waikato, Waikato, New Zealand). All remaining statistical analyses were conducted using standard software (SPSS 23.0; IBM, Chicago, Ill). A two-tailed *P* value less than 0.05 was considered to indicate statistical significance.

3. Results

3.1. Subjective visual image analysis

Subjective visual analysis of the two readers, R1 and R2, for diagnosing MI on CT showed a poor interreader (kappa 0.3) and excellent intrareader agreement (kappa 0.93). Sensitivity for diagnosing MI was highest in ADMIRE strength level 5 image reconstructions for both readers (80% for R1, 60% for R2), while the highest specificity was found at different reconstructions: 95% specificity for R1 in ADMIRE strength level 5 images, and 95% specificity for R2 in FBP images. For comparison, a board-certified Radiologist (R3) had an overall higher sensitivity and specificity than R1 or R2 ranging from 80 to 90% and 100% independent of the reconstruction algorithm. Detailed results are depicted in Table 2.

3.2. Dimension reduction

After excluding 128 of the 308 (42%) TA features per ROI because of ICCs < 0.6, 179 (58%) features remained for further analysis. These remaining features showed an excellent intrareader (ICC 0.9 ± 0.06, range 0.6–0.98) and excellent interreader agreement (ICC 0.8 ± 0.1, 0.72–0.99).

3.3. Decision trees

Different reconstruction algorithms (FBP, ADMIRE strength levels 3, 4, 5) at otherwise fixed settings resulted in four inherently different pruned C4.5 decision trees for classification of patients with MI and healthy controls (Supplementary Fig. 1).

Based on the entire data set, similar performance was observed among all reconstruction algorithms (FBP, ADMIRE strength levels 3–5), with correctly classified instances ranging from 94%–97% (Table 3) and AUCs ranging from 0.94–0.99 (Fig. 2). Slightly lower performance was observed at ADMIRE 3 reconstructions, possibly because of the lower number of leaves (n = 2) in its pruned decision tree.

After splitting the data set into training and test sets, markedly lower performance measures were observed, with overall correctly classified instances ranging from 46%–73% and AUCs ranging from

Table 2
Results from subjective visual image analysis.

Reader	Parameter	FBP	ADMIRE 3	ADMIRE 4	ADMIRE 5
Reader 1	TPR/sensitivity (%)	30	30	50	80
	FPR (%)	30	10	5	5
	TNR/specificity (%)	70	90	95	95
	FNR (%)	70	70	50	20
Reader 2	TPR/sensitivity (%)	30	30	60	60
	FPR (%)	5	15	20	20
	TNR/specificity (%)	95	85	80	80
	FNR (%)	70	70	40	40
Reader 3	TPR/sensitivity (%)	80	90	90	90
	FPR (%)	0	0	0	0
	TNR/specificity (%)	100	100	100	100
	FNR (%)	20	10	10	10

ADMIRE = Advanced modeled iterative reconstruction; FBP = filtered back projection; FNR = false-negative rate; FPR = false-positive rate; TNR = true-negative rate; TPR = true-positive rate.

Table 3
Summary of the machine learning (C4.5 decision tree) results.

Reconstruction Kernel	Data Set	Correctly Classified Instances	Incorrectly Classified Instances	ROC AUC	TN	FP	FN	TP	Sensitivity	Specificity
FBP	Full	97%	3.20%	0.99	19	1	0	11	1	0.95
	Split	46%	54.50%	0.43	4	2	4	1	0.2	0.67
ADMIRE 3	Full	97%	3.20%	0.97	20	0	1	10	0.91	1
	Split	64%	36.40%	0.62	5	1	3	2	0.4	0.83
ADMIRE 4	Full	94%	6.50%	0.95	19	1	1	10	0.8	0.95
	Split	55%	45.50%	0.53	4	2	3	2	0.4	0.67
ADMIRE 5	Full	97%	3.20%	0.99	20	0	1	10	0.91	1
	Split	73%	27.30%	0.65	6	0	3	2	0.4	1

ADMIRE = advanced modeled iterative reconstruction; AUC = area under the curve; FBP = filtered back projection; FN = false negative; FP = false positive; ROC = receiver-operating characteristic; TN = true negative; TP = true positive. All *P*-values of ROC were $P < 0.001$.

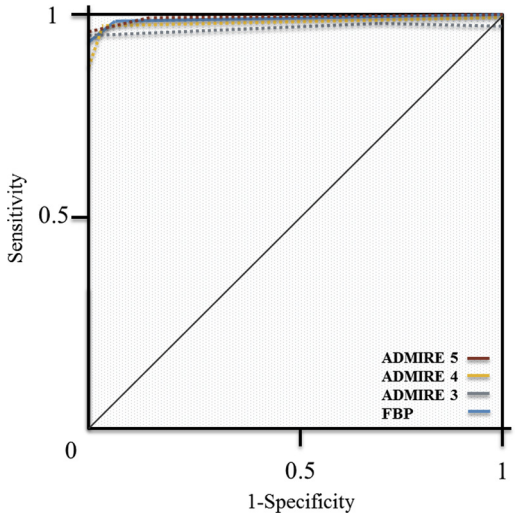

Fig. 2. Receiver-operating characteristic analysis of machine learning–based decision trees on the training set of coronary CTA images reconstructed with filtered back projection (blue), advanced modeled iterative reconstruction (ADMIRE) strength level 3 (gray), ADMIRE strength level 4 (yellow), and ADMIRE strength level 5 (red). *P*-values for all four ROC curves were $P < 0.001$. Note the equally high accuracy for all image reconstruction types when including all cases and controls into the analyses.

0.43–0.65. The lowest performance was observed for FBP images, with successive increases of accuracy for ADMIRE images at higher strength levels (see Table 3).

4. Discussion

This proof-of-principle study shows that TA allows for reproducible analysis of myocardial tissue in contrast-enhanced CT images. While subjective visual analysis of contrast-enhanced CT for the diagnosis of MI has high intrareader agreement, the interreader agreement was overall poor. Furthermore, we showed that iterative reconstruction impacts TA and classification results thereof.

TA represents a data postprocessing tool aimed at disclosing quantitative information contained within medical images, which is an ongoing field of research with applications ranging from lesion detection to clinical outcome prediction. Handling of the resulting data is challenging and often requires machine learning–based algorithms for dimension reduction, feature selection, and outcome classification.

TA in cardiac imaging applications is still relatively rare. Baessler et al. showed the value of TA in cardiac MR imaging for myocardial scar detection [22] and hypertrophic cardiomyopathy [23], and Larroza et al. distinguished old from new MI using MR imaging [24]. Only a few studies thus far have reported the potential of TA for cardiac CT. Antunes et al. showed that TA helps in the characterization of scars in myocarditis using CT [25]. Hinzpeter et al. showed how TA can be used for distinguishing healthy myocardium from acute MI in contrast-enhanced cardiac CT [17], and Mannil et al. indicated the potential of TA for diagnosing acute MI on non–contrast-enhanced CT performed for calcium scoring [11].

Our study adds to the literature the following: i) subjective visual analysis of CT coronary angiography images for the diagnosis of MI shows excellent intrareader but poor interreader agreement; ii) sensitivity and specificity of subjective visual analysis vary considerably among the different image reconstruction types; iii) in comparison to subjective visual image analysis, quantitative TA features are inherently objective and reproducible, and variability is exclusively related to free-hand ROI delineation; iv) there exist considerable differences in machine learning–based decision tree models regarding the relevant TA features when using different image reconstruction types, highlighting the impact of reconstruction algorithm on TA; v) analysis including the entire data set yielded a near-perfect discriminatory power of TA between patients with MI controls for all image reconstruction algorithms, indicating overfitting; and vi) splitting the data set into training and test data to avoid overfitting showed good classification results for the IR technique at the highest strength level.

Gosalia et al. [26] was among the first to describe the potential of contrast-enhanced chest CT for detecting MI. Later studies using ECG-gated cardiac CT acquisitions in the first-pass arterial phase confirmed the ability of CT to diagnose MI [27]. However, the low contrast resolution of CT for diagnosing myocardial abnormalities still is a major drawback when compared with that of the gold standard modality MR imaging. In contrast to the diagnosis of CAD with CT, which has been shown to be heavily dependent on reader experience [28], no study thus far has determined the intra- and interobserver agreement of readers to diagnose MI on CT images. Our study including two readers with experience levels 1 and 2 in cardiovascular imaging confirms this variability also for the diagnosis of areas with hypodense myocardium with CT. The low interreader agreement and the overall better performance of a more experienced reader observed in our study confirms this variability also for the diagnosis of MI in CT. This is important to recognize since sometimes relatively inexperienced radiology residents need to read cardiac CT studies in an after-hour emergency setting.

Image impression of IR images is different from that of FBP images in cardiac applications [29,30], which has been previously objectified by the quantitative parameters noise power spectrum and modulation transfer function [31]. The relatively high intrareader agreement observed in our study is most probably related to personal preferences, being constant among the different image reconstructions for the individual reader. Our study indicates that sensitivity of MI diagnosis improves with higher IR strength levels, but specificity differs among inexperienced readers, being highest in FBP images in one reader and highest at IR strength levels 4 and 5 in the other. It is known that improvements in the objective measures of noise and contrast-to-noise ratio do not necessarily translate into improvements in visual accuracy [32], and an individually preferred image appearance usually does not correspond to the highest strength of IR because of its altered image

appearance [33]. However, in TA, the advantages of IR with reduced noise and increased contrast-to-noise ratio seem to improve the accuracy.

In contrast to subjective preferences, TA is based on objective image information regarding pixel intensities and gray scales. The variability in our study leading to the exclusion of 128 of the 308 TA features because of reduced ICCs is based solely on differences in free-hand ROI delineation of the LV. Machine learning identified different sets of TA features for each individual reconstruction algorithm that were then used in corresponding decision tree classifiers. These findings are in accordance with a recent study of lung tumors by Kim et al. [34], who found that most analyzed TA features, including gray-level co-occurrence matrix (GLCM), were significantly affected by the type of image reconstruction algorithms. Slice thickness was set to 5 mm, as previously shown [17]. Additional variability in TA features according to different scanner types [35], pixel spacing, and matrix size [36] were avoided in our study by using one single CT scanner, identical image reconstruction settings, use of image normalization between the histogram's mean and three standard deviations [19], and rescaling of images according to the pixel spacing values obtained from the DICOM header.

Compared to inexperienced readers, TA showed markedly improved accuracy for detecting MI in cardiac CT images, with best results at highest IR levels. The accurate diagnosis of MI in ADMIRE strength level 5 images was found when combining GLCM (S (5;5) Correlat), run-length matrix (RLM; 135° RLNonUni), and Wavelet (LHs_4, HLs_5, HHs_5) TA features. A detailed description of the meaning of the higher-level TA features is beyond the scope of this manuscript. In brief, GLCM captures the spatial dependence of gray-level values within an image. [37]. RLM is based on computing the number of gray-level runs of various lengths, where a gray level run represents a set of linearly adjacent picture points at a set angle (e.g., 135°) with the same gray-level value [38]. Finally, the discrete wavelet transform is a tool that separates data into different frequency components and then studies each component with resolution matched to its scale [39]. While the subjective image analysis was based on identifying hypoattenuating regions of the myocardium, the machine learning–based decision tree classifier did not identify and did not require histogram-derived features. Instead, it extracted higher-level features depicting micro-architectural changes of the myocardium that are most probably not visible to the human eye. Similar results in different cardiac imaging applications have been reported before [11,17,25].

A common problem in machine learning–based analyses is overfitting. To avoid an unrealistic perfect classification, we split our data into the recommended ratio of 2/3 training data set for decision tree generation and validated the model on the remaining third as a separate testing data set, as previously shown [21]. Classification performance usually is lower when validating on an unseen data set, as seen in our study, which showed an overall lower performance of TA features when splitting the data. Still, our results indicate that TA features perform best for the dichotomic task at hand when using images reconstructed with IR that have the least noise levels and highest signal- and contrast-to-noise ratios.

A potential clinical application of the approach proposed herein would be a clinical decision support system. Machine learning–based TA could be automatically run on the coronary CTA and chest pain CT images with segmented hearts, in parallel to the routine visual analysis by the attending radiologist, thereby potentially helping the reader in pointing out areas in the myocardium that are suspicious for MI. To account for the poor visual interreader reliability an iterative machine learning approach per segment or image would be possible. Such a system could be particularly helpful in emergency situations and for less experienced readers, with the latter showing suboptimal reading performances as indicated by the results of our study.

The following study limitations must be acknowledged. First, this was a retrospective study with inherent limitations. Second, human readers were given only short-axis images for review, while TA was limited to a single image of interest. Third, we included a low number of patients with MI and controls. Due to the low number of patients, we were unable to perform meaningful ROC analyses of the test data set alone. Larger data sets are likely to improve the performance of the supervised decision tree classification and decrease overfitting of the algorithms, as shown in the analysis when testing and using machine learning in the same cases. Certainly, future studies need to include larger sample sizes. While the diagnosis of MI was confirmed clinically and by using catheter coronary angiography, the extent of MI was confirmed using various cross-sectional imaging techniques which might introduce a bias. Finally, our study was performed with only one CT scanner type, similarly to the image reconstruction types. Thus, generalizability of our results need to be proven by future studies, including different CT machines and corresponding image reconstruction algorithms.

In conclusion, our proof-of-principle study indicates the feasibility of TA for the identification of MI in cardiac CTA examinations, showing potential advantages over a visual image analysis of inexperienced readers through its objective and quantitative nature. Furthermore, our study indicates the impact of various image reconstruction algorithms on the results of both subjective and objective image analysis.

Appendix A. Supplementary data

Supplementary material related to this article can be found, in the online version, at doi:https://doi.org/10.1016/j.ejrad.2019.02.037.

References

[1] A.S. Go, D. Mozaffarian, V.L. Roger, E.J. Benjamin, J.D. Berry, et al., American Heart Association Statistics, S. Stroke Statistics, Heart disease and stroke statistics–2014 update: a report from the American Heart Association, Circulation 129 (3) (2014) e28–e292.

[2] K. Thygesen, J.S. Alpert, A.S. Jaffe, M.L. Simoons, B.R. Chaitman, H.D. White, I. Task Force for the Universal Definition of Myocardial, Third universal definition of myocardial infarction, Nat. Rev. Cardiol. 9 (11) (2012) 620–633.

[3] M.W. von Ballmoos, B. Haring, P. Juillerat, H. Alkadhi, Meta-analysis: diagnostic performance of low-radiation-dose coronary computed tomography angiography, Ann. Intern. Med. 154 (6) (2011) 413–420.

[4] M. Task Force, G. Montalescot, U. Sechtem, S. Achenbach, F. Andreotti, C. Arden, A. Budaj, R. Bugiardini, F. Crea, T. Cuisset, C. Di Mario, J.R. Ferreira, B.J. Gersh, A.K. Gitt, J.S. Hulot, N. Marx, L.H. Opie, M. Pfisterer, E. Prescott, F. Ruschitzka, M. Sabate, R. Senior, D.P. Taggart, E.E. van der Wall, C.J. Vrints, E.S.C.Cf.P. Guidelines, J.L. Zamorano, S. Achenbach, H. Baumgartner, J.J. Bax, H. Bueno, V. Dean, C. Deaton, C. Erol, R. Fagard, R. Ferrari, D. Hasdai, A.W. Hoes, P. Kirchhof, J. Knuuti, P. Kolh, P. Lancellotti, A. Linhart, P. Nihoyannopoulos, M.F. Piepoli, P. Ponikowski, P.A. Sirnes, J.L. Tamargo, M. Tendera, A. Torbicki, W. Wijns, S. Windecker, R. Document, J. Knuuti, M. Valgimigli, H. Bueno, M.J. Claeys, N. Donner-Banzhoff, C. Erol, H. Frank, C. Funck-Brentano, O. Gaemperli, J.R. Gonzalez-Juanatey, M. Hamilos, D. Hasdai, S. Husted, S.K. James, K. Kervinen, P. Kolh, S.D. Kristensen, P. Lancellotti, A.P. Maggioni, M.F. Piepoli, A.R. Pries, F. Romeo, L. Ryden, M.L. Simoons, P.A. Sirnes, P.G. Steg, A. Timmis, W. Wijns, S. Windecker, A. Yildirir, J.L. Zamorano, ESC guidelines on the management of stable coronary artery disease: the Task Force on the management of stable coronary artery disease of the European Society of Cardiology, Eur. Heart J. 34 (38) (2013) 2949–3003 2013.

[5] N. Bettencourt, N.D. Ferreira, D. Leite, M. Carvalho, W.D.S. Ferreira, A. Schuster, A. Chiribiri, A. Leite-Moreira, J. Silva-Cardoso, E. Nagel, V. Gama, CAD detection in patients with intermediate-high pre-test probability: low-dose CT delayed enhancement detects ischemic myocardial scar with moderate accuracy but does not improve performance of a stress-rest CT perfusion protocol, JACC Cardiovasc. Imaging 6 (10) (2013) 1062–1071.

[6] L. La Grutta, P. Toia, E. Maffei, F. Cademartiri, R. Lagalla, M. Midiri, Infarct characterization using CT, Cardiovasc. Diagn. Ther. 7 (2) (2017) 171–188.

[7] M. Perazzolo Marra, J.A. Lima, S. Iliceto, MRI in acute myocardial infarction, Eur. Heart J. 32 (3) (2011) 284–293.

[8] C. Delgado Sanchez-Gracian, R. Oca Pernas, C. Trinidad Lopez, E. Santos Armentia, A. Vaamonde Liste, M. Vazquez Caamano, G. Tardaguila de la Fuente, Quantitative myocardial perfusion with stress dual-energy CT: iodine concentration differences between normal and ischemic or necrotic myocardium. Initial experience, Eur Radiol 26 (9) (2016) 3199–3207.

[9] J. Solomon, A. Mileto, J.C. Ramirez-Giraldo, E. Samei, Diagnostic performance of an advanced modeled iterative reconstruction algorithm for low-contrast detectability with a third-generation dual-source multidetector CT scanner: potential for radiation dose reduction in a multireader study, Radiology 275 (3) (2015) 735–745.

[10] A. Euler, B. Stieltjes, Z. Szucs-Farkas, R. Eichenberger, C. Reisinger, A. Hirschmann, C. Zaehringer, A. Kircher, M. Streif, S. Bucher, D. Buergler, L. D'Errico, S. Kopp, M. Wilhelm, S.T. Schindera, Impact of model-based iterative reconstruction on low-contrast lesion detection and image quality in abdominal CT: a 12-reader-based comparative phantom study with filtered back projection at different tube voltages, Eur. Radiol. 27 (12) (2017) 5252–5259.
[11] M. Mannil, J. von Spiczak, R. Manka, H. Alkadhi, Texture analysis and machine learning for detecting myocardial infarction in Noncontrast low-dose computed tomography: unveiling the invisible, Invest. Radiol. 53 (6) (2018) 338–343.
[12] K. Yasaka, H. Akai, M. Nojima, A. Shinozaki-Ushiku, M. Fukayama, J. Nakajima, K. Ohtomo, S. Kiryu, Quantitative computed tomography texture analysis for estimating histological subtypes of thymic epithelial tumors, Eur. J. Radiol. 92 (2017) 84–92.
[13] R.C.J. Beckers, D.M.J. Lambregts, R.S. Schnerr, M. Maas, S.X. Rao, A.G.H. Kessels, T. Thywissen, G.L. Beets, S. Trebeschi, J.B. Houwers, C.H. Dejong, C. Verhoef, R.G.H. Beets-Tan, Whole liver CT texture analysis to predict the development of colorectal liver metastases-A multicentre study, Eur. J. Radiol. 92 (2017) 64–71.
[14] M. Mannil, J. von Spiczak, T. Hermanns, C. Poyet, H. Alkadhi, C.D. Fankhauser, Three-dimensional texture analysis with machine learning provides incremental predictive information for successful shock wave lithotripsy in patients with kidney stones, J. Urol. 200 (4) (2018) 829–836.
[15] R. Goetti, S. Kozerke, O.F. Donati, D. Surder, P. Stolzmann, P.A. Kaufmann, T.F. Luscher, R. Corti, R. Manka, Acute, subacute, and chronic myocardial infarction: quantitative comparison of 2D and 3D late gadolinium enhancement MR imaging, Radiology 259 (3) (2011) 704–711.
[16] M.D. Cerqueira, N.J. Weissman, V. Dilsizian, A.K. Jacobs, S. Kaul, W.K. Laskey, D.J. Pennell, J.A. Rumberger, T. Ryan, M.S. Verani, S. American Heart Association Writing Group on Myocardial, I. Registration for Cardiac, Standardized myocardial segmentation and nomenclature for tomographic imaging of the heart. A statement for healthcare professionals from the Cardiac Imaging Committee of the Council on Clinical Cardiology of the American Heart Association, Int. J. Cardiovasc. Imaging 18 (1) (2002) 539–542.
[17] R. Hinzpeter, M.W. Wagner, M.C. Wurnig, B. Seifert, R. Manka, H. Alkadhi, Texture analysis of acute myocardial infarction with CT: first experience study, PLoS One 12 (11) (2017) e0186876.
[18] P.M. Szczypinski, M. Strzelecki, A. Materka, A. Klepaczko, MaZda–a software package for image texture analysis, Comput. Methods Programs Biomed. 94 (1) (2009) 66–76.
[19] G. Collewet, M. Strzelecki, F. Mariette, Influence of MRI acquisition protocols and image intensity normalization methods on texture classification, Magn. Reson. Imaging 22 (1) (2004) 81–91.
[20] J.R. Landis, G.G. Koch, The measurement of observer agreement for categorical data, Biometrics 33 (1) (1977) 159–174.
[21] K.K. Dobbin, R.M. Simon, Optimally splitting cases for training and testing high dimensional classifiers, BMC Med. Genomics 4 (2011) 31.
[22] B. Baessler, M. Mannil, S. Oebel, D. Maintz, H. Alkadhi, R. Manka, Subacute and chronic left ventricular myocardial scar: accuracy of texture analysis on nonenhanced cine MR images, Radiology 286 (1) (2018) 103–112.
[23] B. Baessler, M. Mannil, D. Maintz, H. Alkadhi, R. Manka, Texture analysis and machine learning of non-contrast T1-weighted MR images in patients with hypertrophic cardiomyopathy-preliminary results, Eur. J. Radiol. 102 (2018) 61–67.
[24] A. Larroza, A. Materka, M.P. Lopez-Lereu, J.V. Monmeneu, V. Bodi, D. Moratal, Differentiation between acute and chronic myocardial infarction by means of texture analysis of late gadolinium enhancement and cine cardiac magnetic resonance imaging, Eur. J. Radiol. 92 (2017) 78–83.
[25] S. Antunes, A. Esposito, A. Palmisanov, C. Colantoni, F. de Cobelli, A. Del Maschio, Characterization of normal and scarred myocardium based on texture analysis of cardiac computed tomography images, Conf. Proc. IEEE Eng. Med. Biol. Soc. 2016 (2016) 4161–4164.
[26] A. Gosalia, L.B. Haramati, M.P. Sheth, H. Spindola-Franco, CT detection of acute myocardial infarction, AJR Am. J. Roentgenol. 182 (6) (2004) 1563–1566.
[27] K. Nikolaou, A. Knez, S. Sagmeister, B.J. Wintersperger, P. Boekstegers, G. Steinbeck, M.F. Reiser, C.R. Becker, Assessment of myocardial infarctions using multidetector-row computed tomography, J. Comput. Assist. Tomogr. 28 (2) (2004) 286–292.
[28] F. Pugliese, M.G. Hunink, K. Gruszczynska, F. Alberghina, R. Malago, N. van Pelt, N.R. Mollet, F. Cademartiri, A.C. Weustink, W.B. Meijboom, C.L. Witteman, P.J. de Feyter, G.P. Krestin, Learning curve for coronary CT angiography: what constitutes sufficient training? Radiology 251 (2) (2009) 359–368.
[29] T. Gassenmaier, I. Distelmaier, A.M. Weng, T.A. Bley, T. Klink, Impact of advanced modeled iterative reconstruction on interreader agreement in coronary artery measurements, Eur. J. Radiol. 94 (2017) 201–208.
[30] M. Karolyi, B. Szilveszter, M. Kolossvary, R.A. Takx, C. Celeng, A. Bartykowszki, A.L. Jermendy, A. Panajotu, J. Karady, R. Raaijmakers, W. Giepmans, B. Merkely, P. Maurovich-Horvat, Iterative model reconstruction reduces calcified plaque volume in coronary CT angiography, Eur. J. Radiol. 87 (2017) 83–89.
[31] F.A. Mieville, F. Gudinchet, F. Brunelle, F.O. Bochud, F.R. Verdun, Iterative reconstruction methods in two different MDCT scanners: physical metrics and 4-alternative forced-choice detectability experiments–a phantom approach, Phys. Med. 29 (1) (2013) 99–110.
[32] D.B. Husarik, D. Marin, E. Samei, S. Richard, B. Chen, T.A. Jaffe, M.R. Bashir, R.C. Nelson, Radiation dose reduction in abdominal computed tomography during the late hepatic arterial phase using a model-based iterative reconstruction algorithm: how low can we go? Invest. Radiol. 47 (8) (2012) 468–474.
[33] F. Morsbach, L. Desbiolles, R. Raupach, S. Leschka, B. Schmidt, H. Alkadhi, Noise texture deviation: a measure for quantifying artifacts in computed tomography images with iterative reconstructions, Invest. Radiol. 52 (2) (2017) 87–94.
[34] H. Kim, C.M. Park, M. Lee, S.J. Park, Y.S. Song, J.H. Lee, E.J. Hwang, J.M. Goo, Impact of reconstruction algorithms on CT radiomic features of pulmonary tumors: analysis of intra- and inter-reader variability and inter-reconstruction algorithm variability, PLoS One 11 (10) (2016) e0164924.
[35] D. Mackin, X. Fave, L. Zhang, D. Fried, J. Yang, B. Taylor, E. Rodriguez-Rivera, C. Dodge, A.K. Jones, L. Court, Measuring computed tomography scanner variability of radiomics features, Invest. Radiol. 50 (11) (2015) 757–765.
[36] V. Kumar, Y. Gu, S. Basu, A. Berglund, S.A. Eschrich, M.B. Schabath, K. Forster, H.J. Aerts, A. Dekker, D. Fenstermacher, D.B. Goldgof, L.O. Hall, P. Lambin, Y. Balagurunathan, R.A. Gatenby, R.J. Gillies, Radiomics: the process and the challenges, Magn. Reson. Imaging 30 (9) (2012) 1234–1248.
[37] R.M. Haralick, K. Shanmugam, I. Dinstein, Textural features for image classification, IEEE Trans. Syst. Man Cybern. Syst. 3 (6) (1973) 610–621.
[38] X. Tang, Texture information in run-length matrices, IEEE Trans. Image Process. 7 (11) (1996) 1602–1609.
[39] M. Kociołek, A. Materka, M. Strzelecki, P.M. Szczypinski, Discrete wavelet transform- derives features for digital image texture analysis, Proc. of Internation Conference on Signals and Electronic Systems, (2001), pp. 163–168.